Strong room-temperature photoluminescence of β-crystalline Ta_2O_5 nanobrick arrays

Yuan-Ron Ma, Jin-Han Lin, Wei-Der Ho, and Rupesh S. Devan

Department of Physics, National Dong Hwa University, Hualien 97401, Taiwan, Republic of China,
ronma@mail.ndhu.edu.tw

ABSTRACT

We analyzed the structural and photoluminescence properties of a new morphological form, stacking Ta_2O_5 nanobrick arrays that were synthesized by hot filament metal-oxide vapor deposition. Field-emission scanning electron microscopy showed the stacking Ta_2O_5 nanobricks to be arranged in a large-area array, on average ~20.7 nm wide. X-ray diffractometery showed the stacking Ta_2O_5 nanobricks to be the orthorhombic (β) phase, assigned to the space group $P2_12_12$. Photoluminescence spectra showed very strong green-light emissions, which emerged from the trap-levels of the oxygen vacancies within the Ta_2O_5 bandgap. One of the trap-levels, called the midgap state, can provide a very intense 566.3 nm emission with 44.0 % and 69.8 % of the intensity of the incident 486.8 and phonon-assisted 499.5 nm lasers, respectively, a strong indication that the stacking Ta_2O_5 nanobricks are good room-temperature visible-light emitters.

Keywords: Ta_2O_5, nanobricks, x-ray diffraction (XRD), photoluminescence (PL), room-temperature.

1 INTRODUCTION

Over the past few decades, researchers have been engaged in the study of metal-oxide thin-films and bulk materials. The high dielectric constant values as well as the steady thermal and chemical properties [1-5] of Ta_2O_5 thin films, as compared to those of SiO_2 thin films [2-4,6-7], make them good candidate materials for capacitors to be integrated into memory devices and for advanced electronic packing applications. Ta_2O_5 films also offer a wide-range of refractive-index adjustments [8] for integrated optical circuits, high-quality antireflection properties for solar cells [9-10], and better ionic conductivity for electrochromic devices (such as the chromogenic glazing in windows and large-scale information displays [11-12]). In addition, Ta_2O_5 is a good thermochromic material; its optical properties can be altered by simply elevating the temperature [13]. Hence, Ta_2O_5 films have potential for use in thermochromic 'smart windows', display devices [14-16], and many other similar applications necessitating electrochromic capabilities [17-18].

The crystalline structures of Ta_2O_5 are complicated, but the structures are based only on a network of TaO_6 octahedra and TaO_7 pentagonal bipyramids [19-20] with shared oxygen atoms. Specifically, Ta_2O_5 consists of only two polyhedral building blocks, TaO_6 octahedra and TaO_7 pentagonal bipyramids. This is similar to SiO_2, where amorphous or crystalline structures of SiO_2 are composed of only one type of building block, the SiO_4 tetrahedron. Oxygen (O) is easily volatilized in the complicated structures of Ta_2O_5, thereby yielding many types of oxygen vacancies. Note that although oxygen vacancies are the most predominant type of defect in Ta_2O_5, they are located at only two sites, the in-plane and the cap [19-20]. Each oxygen vacancy leaves one or two dangling bonds close to the vacancy location and donates two electrons. The dangling bonds can give rise to electronic states within the bandgap, which are able to trap excited electrons. This creates many trap-levels (electronic states) within the bandgap of Ta_2O_5. There is a large variety of in-plane and cap oxygen-vacancy sites that occur at the complex interfacial intersections of TaO_6 octahedra and the TaO_7 pentagonal bipyramids, and more complex interfacial intersections can supply more trap-levels. When the trapped electrons are released from the trap-levels to the ground state, varying wavelengths of visible light are emitted. Therefore, the presence of oxygen vacancies is expected to make Ta_2O_5 an *n*-type semiconductor and is important to play a strong role in the photoluminescence (PL) emissions of Ta_2O_5.

In this study, we synthesized large-scale arrays of stacking Ta_2O_5 nanobricks via hot-filament metal-oxide vapor deposition. The development of the hot-filament metal-oxide vapor deposition technique is very significant, because it can be used to synthesize a variety of nanostructures with different morphologies and crystalline traits [19,21-24] This development has opened up a new field in nanotechnology leading to the discovery of the dependence of electrical, thermal transport and mechanical properties on dimensionality and size reduction. The structural morphology and size distribution of the stacking Ta_2O_5 nanobricks were examined through field-emission scanning electron microscopy (FESEM). X-ray diffractometery (XRD) showed the crystalline structure of the stacking Ta_2O_5 nanobricks. PL spectroscopy is a well-developed optical tool for the inspection of semiconductor materials and devices for impurities and defects. Our room-temperature PL spectra showed very strong green-light emissions. For example, the intensity of the green-light emission of 566.3 nm, which emerged from the midgap trap-level, was about 44.0 % and 69.8 % that of the incident 486.8 and phonon-assisted 499.5 nm lasers, respectively.

The results are a good indication that the stacking Ta_2O_5 nanobricks are effective visible light emitters at room temperature, consequently confirming the viability of a large-scale array of these stacking Ta_2O_5 nanobricks as a potential candidate material for the fabrication of optoelectronic nanodevices, such as light emitting diodes (LEDs) and laser diodes (LDs).

2 EXPERIMENTAL METHODS

Large-scale arrays of stacking Ta_2O_5 nanobricks were synthesized using the hot filament metal-oxide vapor deposition technique. Clean tantalum (Ta) wires (99.98 % pure) with a diameter of 1 mm were passed through a pure graphite disc fixed to two supporting Cu electrodes mounted in a vacuum chamber. Once the pressure of the vacuum chamber was pumped down to 1×10^{-2} Torr, the Ta wire was heated to ~1800 ^{o}C for 10 min to generate hot tantalum vapor. When the hot tantalum vapor encountered the residual oxygen (or leaking air), a metal-oxide vapor arose which condensed into nanobricks on the cold Si wafer substrates. The substrates were placed on a graphite disc holder (~ 3 mm above the Ta-wires). Characterization of the as-synthesized large-area arrays of stacking Ta_2O_5 nanobricks thus produced was carried out with a field emission scanning electron microscope (JEOL JSM-6500F). Structural analysis of the stacking Ta_2O_5 nanobricks was carried out using an x-ray diffractometer (Philips X'Pert PRO) with Cu Kα radiations (λ=1.541 Å). The PL properties of the stacking Ta_2O_5 nanobricks were studied by scanning near-field optical microscopy (WITec, Alpha300 S) with an excitation laser of 486.8 nm (CVI Melles Griot 43 series, Ar ion laser, model 35-LAL-415-208).

3 RESULTS AND DISCUSSION

The surface morphology of the large-scale array of stacking Ta_2O_5 nanobricks can be seen in the FESEM image in Fig. 1(A). The stacking Ta_2O_5 nanobrick array is very compact, but its textural boundaries are clearly visible. The array contains ~1630 nanobricks per micrometer square. Various widths of the stacking Ta_2O_5 nanobricks all are smaller than 50 nm. The XRD patterns reveal details of the crystalline structures. Fig. 1(B) displays the XRD spectra of the stacking Ta_2O_5 nanobricks. From the diffraction peaks it can be seen that the large-area array of the stacking Ta_2O_5 nanobricks consists of only the orthorhombic (β) phase. The orthorhombic (β) phase is assigned to the space group $P2_12_12$ with lattice constants of a = 0.6198 nm, b = 4.029 nm, c = 0.3880 nm and $\alpha = \beta = \gamma = 90^{\circ}$ (JCPDS 25-0922). The diffraction peaks (indicated by β) at 2θ = 22.9º, 28.2º, 28.5º, 28.7º, 28.8º, 28.9º, 37.1º, 37.2º, 38.4º, 44.7º, 59.8º, 60.1º, 60.4º, and 61.4º, respectively correspond to the (001), (1 11 0), (141), (200), (210), (081), (201), (211), (1 12 1), (2 15 0) or (340), (2 20 1), (410), (420), and (2 22 1) lattice planes.

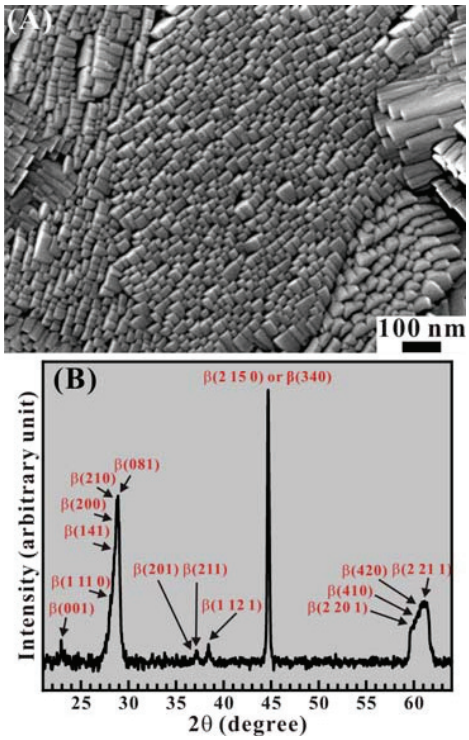

Fig.1. (A) FESEM image and (B) XRD spectrum of large-scale arrays of stacking Ta_2O_5 nanobricks

In previous experimental studies [25-33], trap-levels and shallow centers of oxygen vacancies within the bandgap of Ta_2O_5 have been observed. However, some theoretical studies [19-20,34] predict more trap-levels and shallow centers to be created within the bandgap. Therefore, it is of great interest to inspect the PL performance of the stacking Ta_2O_5 nanobricks. PL spectroscopy is a powerful optical tool that can be used to probe the impurities and defects in semiconductor materials. Fig. 2 shows the strong room-temperature PL spectra of the large-area array of stacking Ta_2O_5 nanobricks. The two sharp peaks at 486.8 and 499.5 nm (labeled by **1** and **2**, respectively) in Fig. 2(A) correspond to the incident and phonon-assisted lasers. Their full widths at half maxima (FWHMs) are only 0.9 nm. The very narrow FWHMs verify that the two sharp peaks represent laser emissions. As known, we synthesized the stacking Ta_2O_5 nanobricks on Si substrates. When the incident 486.8 nm laser impacts on the Si substrate, strong Si Raman scattering (or phonon effect) occurs. Here, some of the incident 486.8 nm laser (labeled by **1**) was absorbed by Ta_2O_5 samples, but some passed through the Ta_2O_5 samples and impacted on the Si substrate. Thus, the incident laser can be adsorbed to induce multiple lasers, which are called phonon-assisted lasers. The phonon-assisted 499.5 nm lasers (labeled by **2**) have intense intensity, because it corresponds to the Si Raman band of ~520 cm^{-1}.

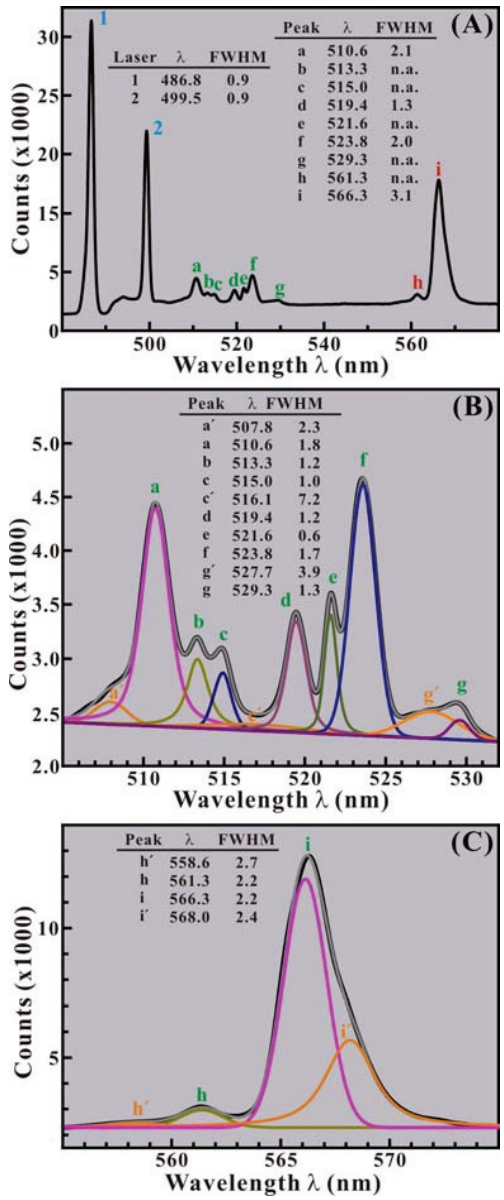

Fig. 2. (A) Room-temperature PL spectra of the stacking Ta_2O_5 nanobricks. The PL spectra in (B) and (C) are decomposed via partial Gaussian and Lorentz curve fittings.

In addition, there are two emission spectral bands located at green-light wavelengths ranging from 510 to 530 nm and from 560 to 570 nm. The first emission band consists of seven green-light emissions of 510.6 (labeled by **a**), 513.3 (labeled by **b**), 515.0 (labeled by **c**), 519.4 (labeled by **d**), 521.6 (labeled by **e**), 523.8 (labeled by **f**), and 529.3 (labeled by **g**). The second emission band contains two green-light emissions of 561.3 (labeled by **h**), and 566.3 (labeled by **i**) nm. Only the four **a**, **d**, **f**, and **i** peaks have indisputable FWHMs of 2.1, 1.3, 2.0, and 3.1 nm. Apparently, the **i** peak receives strong intensity, which is 44.0 % and 69.8 % that of the laser **1** and **2** peaks, indicating that the stacking Ta_2O_5 nanobrick array can generate very strong green-light emissions. The remaining **a**, **d**, and **f** peaks also have very high intensities, which are 15.1 % and 24.0 %, 11.9 % and 18.9 %, and % 15.8 and 25.0 % those of the lasers **1** and **2** peaks, respectively. The first emission band can be decomposed with partial Gaussian and Lorentz curve fittings. The results of decomposition are shown in Fig. 2(B). After decomposition, there are three more peaks found at 507.8 (labeled by **a′**), 516.1 (labeled by **c′**), and 527.7 (labeled by **g′**) nm with the FWHMs of 2.3, 7.2, and 3.9 nm, respectively. The **a**, **b**, **c**, **d**, **e**, **f**, and **g** peaks reach their genuine FWHMs of 1.8, 1.2, 1.0, 1.2, 0.6, 1.7, 1.3 nm. The second emission band is also decomposed using partial Gaussian and Lorentz curve fittings, with the decomposition results being shown in Fig. 2(C). After decomposition, there are two more peaks discovered at 558.6 (labeled by **h′**) and 568.0 (labeled by **i′**) nm with FWHMs of 2.7 and 2.4 nm. The **h** and **i** peaks reach their authentic FWHMs of 2.2 nm. In brief, the PL results demonstrate that the large-area array of the stacking Ta_2O_5 nanobricks can provide numerous and various trap-levels within the bandgap, due to variations in the number of types of oxygen vacancies on the surfaces of the large-area array.

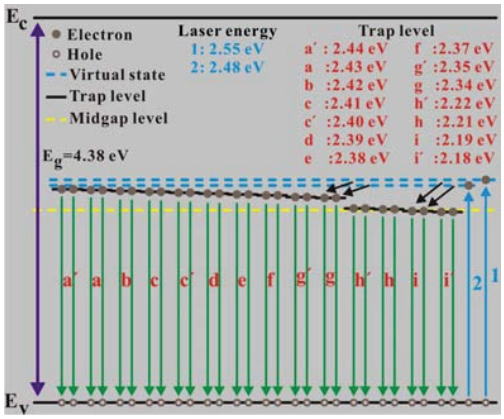

Fig. 3. Schematic diagram of the trap-level emissions of the stacking Ta_2O_5 nanobricks.

Fig. 3 shows a schematic diagram of the room-temperature trap-level emissions of the stacking Ta_2O_5 nanobrick array. The schematic representation of the various trap-levels within the bandgap of Ta_2O_5 helps to explain the room-temperature PL results in Fig. 2. The **a′**, **a**, **b**, **c**, **c′**, **d**, **e**, **f**, **g**, **g**, **h′**, **h**, **i**, and **i′** peaks correspond to oxygen vacancy trap-levels of 2.44, 2.43, 2.42, 2.41, 2.40, 2.39, 2.38, 2.37, 2.35, 2.34, 2.22, 2.21, 2.19 and 2.18 eV, respectively. Electrons in the valence band are excited by two laser lights with wavelengths of 486.8 and 499.5 nm to the virtual states of 2.55 and 2.48 eV. The excited electrons undergo nonradiative transitions to the varying trap-levels, implying that at room temperature they are naturally trapped by the dangling bonds around the oxygen vacancies. When the trapped electrons return to the valence band, they

emit photons (i.e., PL) to release photonic energy during the radiative transitions. Since the **i** peak is large, the trap level of 2.19 eV corresponds to the midgap state [25-33]. The midgap state implies that the energy bandgap of the stacking Ta_2O_5 nanobrick array is ~ 4.38 eV, which agrees with previous results [27,35-36]. The stacking Ta_2O_5 nanobrick array has a wide bandgap of ~4.38 eV making it more suitable for ultraviolet (UV) and blue optoelectronic applications. The stacking Ta_2O_5 nanobrick arrays not only provide green-light emissions, but also UV-light and blue-light emissions. The next stage will be the fabrication of electroluminescent nanodevices from them, such as light emitting diodes (LEDs) and laser diodes (LDs), when suitable *p*-type materials are found for the *n*-type stacking Ta_2O_5 nanobrick array.

4 CONCLUSION

We scrutinized the structural and electronic properties of a large-area stacking Ta_2O_5 nanobrick array synthesized using hot filament metal vapor deposition. The stacking Ta_2O_5 nanobricks were about 20.7 nm wide, and were composed of the orthorhombic (β) phase only at room temperature. The stacking Ta_2O_5 nanobrick arrays provided very strong green-light emissions at room temperature, which emerged from the numerous oxygen vacancies of the large-area array surfaces. The numerous oxygen of the stacking Ta_2O_5 nanobrick large-scale array arrangement make it a strong candidate for optoelectronic nanodevices, such as light emitting diodes (LEDs) and laser diodes (LDs).

5 ACKNOWLEDGEMENT

The authors would like to thank the National Science Council of the Republic of China for their financial support of this research under Contract Nos. NSC-97-2112-M- 259-005-MY2 and NSC-96-2811-M-259-004.

REFERENCES

[1]/ S. C. Sun and T. F. Chen, *IEEE Electron. Device. Lett*. 1996, **17,** 355-357.
[2]/ C. Chaneliere, J. L. Autran, R. A. B. Devine and B. Balland, *Mater. Sci. Eng. R-Rep.* 1998, **22,** 269-322.
[3]/ J. P. Chang, M. L. Steigerwald, R. M. Fleming, R. L. Opila and G. B. Alers, *Appl. Phys. Lett.*1999, **74,** 3705-3707.
[4]/ G. Lucovsky, G. B. Rayner and R. S. Johnson, *Microelectron. Reliab.* 2001, **41,** 937-945.
[5]/ S. D. Kim, *Curr. Appl. Phys.* 2007, **7,** 124-134
[6]/ M. S. Mattsson, G. A. Niklasson, K. Forsgren and A. Hårsta. *J. Appl. Phys.* 1999, **85,** 2185-2191.
[7]/ S. Zafar, A. Kumar, E. Gusev and E. Cartier, *IEEE Trans. Device Mater. Reliab.* 2005, **5,** 45-64.
[8]/ H. Terui, and M. Kobayashi, *Appl. Phys. Lett.* 1978, **32,** 666-668.
[9]/ D. Bouhafs, A. Moussi, A. Chikouche and J. M. Ruiz, *Sol. Energy. Mater. Sol. Cells*. 1998, **52** 79-93.
[10]/M. Cid, N. Stem, C. Brunetti, A. F. Beloto and C. A. S. Ramos, *Surf. Coat. Technol.* 1998, **106,** 117-120.
[11]/M. J. Duggan, T. Saito and T. Niwa, *Solid. State. Ion.* 1993, **62,** 15-20.
[12]/C. Corbella, M. Vives, A. Pinyol, I. Porqueras, C. Person and E. Bertran, *Solid. State. Ion.* 2003, **165,** 15-22.
[13]/R. S. Devan, W.-D. Ho, J.-H. Lin, S. Y. Wu, Y.-R. Ma, P.-C. Lee and Y. Liou, *Cryst. Growth. Design.* 2008, **8,** 4465-4468.
[14]/C. Sella, M. Maaza, O. Nemraoui, J. Lafait, N. Renard and Y. Sampeur, *Surf. Coat. Technol.* 1998, **98,** 1477-1482.
[15]/N. Ozer and C. M. Lampert, *Sol. Energy. Mater. Sol. Cells.* 1998, **54,** 147-156.
[16]/C. C. Liao, F. R. Chen and J. J. Kai, *Sol. Energy. Mater. Sol. Cells.* 2007, **91,** 1282-1288.
[17]/J. S. Hale, M. DeVries, B. Dworak and J. A. Woollam, *Thin Solid Films* 1998, **313-314,** 205-209.
[18]/H. Yoshimura and N. Koshida, *Appl. Phys. Lett.* 2006, **88,** 093509.
[19]/H. Sawada and K. Kawakami, *J. Appl. Phys.* 1999, **86**, 956-959.
[20]/R. Ramprasad, *J. Appl. Phys.* 2003, **94,** 5609-5612.
[21]/Y.-R. Ma, C.-M. Lin, C.-L. Yeh and R.-T. Huang, *J. Vac. Sci. Technol. B* 2005, **23,** 2141-2145.
[22]/L. Kumari, Y.-R. Ma, C.-C. Tsai, Y.-W. Lin, S. Y. Wu, K.-W. Cheng and Y. Liou, *Nanotechnology* 2007, **18,** 115717.
[23]/L. Kumari, J.-H. Lin and Y. -R. Ma, *Nanotechnology* 2007, **18,** 295605.
[24]/L. Kumari, J.-H. Lin and Y. -R. Ma, *J. Phys. Condens. Matter.* 2007, **19,** 406204.
[25]/J. H. III Thomas, *Appl. Phys. Lett.* 1973, **22,** 406-408.
[26]/J. H. III Thomas, *J. Appl. Phys.* 1974, **45,** 835-842.
[27]/J. H. III. Thomas, *J. Appl. Phys.* 1974, **45,** 5349-5355.
[28]/S. Seki, T. Unagami and B. Tsujiyama, *J. Vac. Sci. Technol. A* 1983, **1,** 1825-1830.
[29]/W. S. Lau, L. Zhong, A. Lee, C. H. See, T. Han, N. P. Sandler and T. C. Chong, *Appl. Phys. Lett.* 1997, **71,** 500-502.
[30]/W. S. Lau, L. L. Leong, T. J. Han, and N. P. Sandler, *Appl. Phys. Lett.*2003, **83,** 2835-2837.
[31]/M. M. Zhu, Z. J. Zhang and W. Miao, *Appl. Phys. Lett.* 2006, **89,** 021915.
[32]/H. Shin, S. Y. Park, S. T. Bae, S. Lee, K. S. Hong and H. S. Jung, *J. Appl. Phys.* 2008, **104,** 116108.
[33]/W. Miao, M. M. Zhu, Z. C. Li and Z. Zhang, *J. Mater. Trans.* 2008, **49,** 2288-2291.
[34]/B. R. Sahu and L. Kleinman, *Phys. Rev. B* 2004, **69,** 165202.
[35]/Y. L. Chueh, L. J. Chou and Z. L. Wang, *Angew. Chem-Int. Edit.* 2006, **45,** 7773-7778.
[36]/J. Robertson, *J. Vac. Sc. Technol. B* 2000, **18,** 1785-1791.